J. Fluid Mech. (1999), *vol.* 394, *pp.* 357–377. Printed in the United Kingdom

Flow structure produced by the interaction and merger of a pair of co-rotating wing-tip vortices

By WILLIAM J. DEVENPORT, CHRISTINE M. VOGEL AND JEFFERY S. ZSOLDOS

Department of Aerospace and Ocean Engineering, Virginia Polytechnic Institute and State University, 215 Randolph Hall, Blacksburg, VA 24061, USA

(Received 12 January 1998 and in revised form 24 February 1999)

Experiments have been performed to study the co-rotating wing-tip vortex pair produced by a pair of rectangular wings in a split-wing configuration. Detailed measurements made in cross-sections upstream and downstream of merger reveal, for the first time, the complex turbulence structure of this flow. The vortices spiral around each other and merge some 20 chordlengths downstream of the wings. As merger is approached the vortices lose their axisymmetry – their cores develop lopsided tangential velocity fields and the mean vorticity field is convected into filaments. The cores also become part of a single turbulence structure dominated by a braid of high turbulence levels that links them together. The braid, which quite closely resembles the structure formed between adjacent spanwise eddies of transitional mixing layers, grows in intensity with downstream distance and extends into the vortex cores. Unlike a single tip vortex, the unmerged cores appear turbulent.

The merging of the vortices wraps the cores and the flow structure that surrounds them into a large turbulent region with an intricate double spiral structure. This structure then relaxes to a closely axisymmetric state. The merged core appears stable and develops a structure similar to the laminar core of a vortex shed from a single wing. However, the turbulent region formed around the vortex core during the merger process is much larger and more axisymmetric than that found around a single wing-tip vortex.

1. Introduction

The extensive literature relevant to wing-tip vortices includes several studies devoted to the interaction of equal-strength co-rotating pairs. Brandt & Iversen (1977), Bilanin, Snedeker & Teske (1976) and Bilanin *et al.* (1977*a*) established the basic features of this flow through low-Reynolds-number visualizations of vortices generated by pairs of unswept rectangular wings. The wings were placed tip-to-tip by mounting them on opposite or adjacent walls of a rectangular test section – configurations we shall refer to as the split wing and perpendicular wing respectively. With the wings at equal and opposite angles of attack, equal-strength co-rotating tip vortices are formed that spiral around each other under their mutual induction and ultimately merge to form a single vortex. These authors observed some interesting details of this process – the initially laminar appearance of the unmerged vortex cores, the distortion of the regions of smoke containing the cores and rapid changes in the angular position of the vortex cores as merger is approached, the generation of unsteadiness during the

merger process, and the formation of a double-spiral structure in the smoke patterns downstream of merger that penetrated quite deeply into the new core.

Unfortunately, there have been relatively few quantitative measurements to relate these observations to physical structure in the velocity or turbulence fields. Measurements upstream of merger are particularly rare. The studies of Brandt & Iversen (1977) and Iversen *et al.* (1979) include a few hot-wire profiles measured upstream and downstream of merger in the wake of a perpendicular wing configuration. Smits & Kummer (1985) present similar measurements for a split-wing configuration. These data show some reduction in the peak tangential velocity and change in the shape of the tangential velocity profile as a consequence of merger. Smits & Kummer's results also show a reduction in the axial velocity deficit at the vortex centre. Iversen *et al.* and Smits & Kummer also present turbulence profiles measured through the cores. However, without quantitative documentation of the effects of any vortex wandering – the low-frequency fluctuations in vortex position that can add a large inactive component to velocity fluctuations measured at a fixed point – it is difficult to assess the significance of the high turbulence levels ($\sim$10%) they recorded near the centre of the merged and unmerged vortices. Corsiglia, Iversen & Orloff (1978) attempted to document the mean flow structure produced by a perpendicular-wing configuration using a laser Doppler anemometer with conditional averaging to eliminate wandering effects, but seeding problems and uncertainty obscured much of the structure they were attempting to reveal. Using heat to trace the evolution of the vortices through the merger process, Smits & Kummer concluded that fluid from the two vortices mixes rapidly during merger – an observation apparently at odds with the fine double-spiral structures observed by Bilanin *et al.* (1976, 1977*a*) and Brandt & Iversen (1977).

Measurements downstream of merger in split-wing vortex flows have been made by Hoffmann & Joubert (1963), Poppleton (1971), Phillips & Graham (1984) and Bandyopadhyay, Stead & Ash (1991). In all but the first of these studies the wing tips were separated by a centrebody. These authors were interested in the split wing as a single trailing vortex generator and did not attempt to document the co-rotating vortex pair from which this structure forms. However, a few of their results appear to show remnants of this history. Bandyopadhyay *et al.*'s flow visualizations 40 chordlengths downstream of their split wing show a helical vortex pair wound around the centre of the flow. Phillips & Graham's cases C and D show oscillatory $\overline{uv_r}$ profiles in the merged vortex that decay fairly rapidly with distance downstream, possibly consistent with a double-spiral structure formed during the merger process. The downstream development of the merged vortex is visible to some extent in the results of Poppleton and Phillips & Graham. They show the decay of the mean velocity field of the vortex to be very gradual – suggesting that it has a stable structure. Phillips & Graham and Bandyopadhyay *et al.* also made turbulence measurements that showed substantial velocity fluctuations in the merged vortex core that decay with downstream distance. Bandyopadhyay *et al.*'s results also show non-isotropic ($\overline{v_r^2} \neq \overline{v_\theta^2}$) velocity fluctuations at the vortex centre. It has been known since the work of Hoffmann & Joubert (1963) that the wandering of a merged vortex produced by a split-wing configuration is minimal. It is therefore often assumed (but, as far as we are aware, not quantitatively verified) that such measurements are free from substantial wandering effects.

Further insight into the vortex interaction process may perhaps be gleaned from computational studies of two-dimensional vortex pairs. Point-vortex calculations by Rossow (1977*a*, *b*) and finite difference calculations by Steger & Kutler (1977) both show the distortion of a two-dimensional vortex core into an ellipse by the strain rate

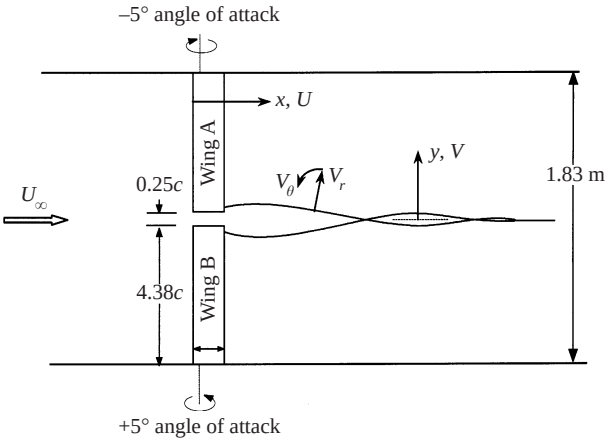

FIGURE 1. Schematic of the wind-tunnel test section showing the 0.203 m chord NACA 0012 half-wings and coordinate systems. Coordinate z and velocity component W are measured out of the paper from the quarter-chord lines of the wings.

field of a co-rotating neighbour – a result originally predicted theoretically by Moore & Saffman (1971). Similar behaviour has been seen by Christiansen & Zabusky (1973) and others in vortex-street simulations. Rossow and Steger & Kutler's work, in conjunction with later studies by Melander, Zabusky & McWilliams (1988) also reveal some of the details of the two-dimensional merger process. Melander *et al.* describe this flow as seen from a frame of reference rotating with the unmerged vortex cores in which a band of streamlines is seen that encompasses both vortex centres – dubbed the exchange band. Vorticity that extends beyond this band becomes convected into filaments that trail behind the orbiting cores. The filaments induce velocities on the vortex cores that then push them together. The subsequent merger winds the filaments into a double-spiral structure. Laminar vortex merger in two dimensions has also been studied computationally by a number of other workers, including Overman & Zabusky (1982) and Dritschel (1995) and others cited therein, because of its relevance to understanding the interaction of eddies in turbulence. Turbulent calculations, using a second-order Reynolds stress closure, have been performed by Bilanin, Teske & Williamson (1977*b*). They initiated their calculation with axisymmetric turbulence stress fields centred on the separate vortex cores, but found that turbulence rapidly formed in a strip running between the co-rotating vortices. This turbulence then appears to end up at the centre of the merged core.

While these papers do give valuable insight into the physics of co-rotating tip vortex pairs and their merger, much of the information needed for a full understanding is missing. There have, for example, been no low-uncertainty measurements of the cross-sectional turbulence structure, and thus little is known about the form of this structure or its evolution through the merger process. There have been no comparisons between the turbulence structure of the merged or unmerged vortices with that of a single wing-tip vortex, nor quantitative measurements of vortex wandering in this type of flow.

The objective of the present paper is to provide some of this missing information. Detailed mean velocity and turbulence measurements been made in a co-rotating vortex pair generated using a split-wing configuration (figure 1) are reported. Comparisons are made with the single wing-tip vortex studied by Devenport *et al.* (1996, hereafter referred to as DLRF), generated using the present configuration but with

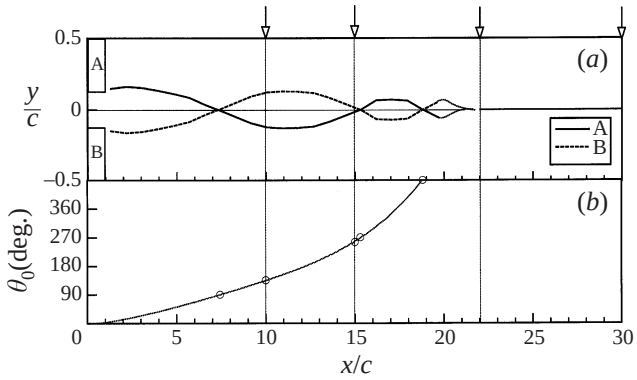

FIGURE 2. Vortex core trajectories inferred from Zsoldos' (1992) helium-bubble flow visualizations and hot-wire velocity measurements. Arrows show velocity-measurement locations. (*a*) Core locations, (*b*) angle between line joining vortex centres and *y*-axis.

one of the half-wings removed. This comparison enables effects associated with interactions between the co-rotating vortices to be distinguished from those associated with individual vortex development. Similar comparisons are made with the results of Devenport, Zsoldos & Vogel (1997, hereafter referred to as DZV) who studied the turbulence structure of a pair of equal-strength counter-rotating vortices generated using the present configuration but with both wings set at the same angle of attack.

2. Apparatus and instrumentation

Most of the apparatus and instrumentation was identified to that used by DLRF and DZV and is thus only briefly reviewed here. Measurements were taken in the Virginia Tech Stability Wind Tunnel. This facility produces a low-turbulence (<0.1%) closely uniform flow through its 1.83 m square, 7.33 m long test section. Vortices were generated using two identical half-wings mounted tip to tip just downstream of the test section entrance, figure 1. Both had a rectangular planform and NACA 0012 section, a chordlength c of 0.203 m and an effective half-span of 0.88 m. Both were equipped with distributed-roughness boundary-layer tips, see DZV. All measurements were made at a chord Reynolds number $Re_c = 260\,000$ corresponding to a free-stream velocity U_∞ of about 20 m s^{-1}.

Helium bubble flow visualizations (Zsoldos 1992) were used to set the angles of attack and separation distance between the wing tips and to choose locations for velocity measurements. With the wings at equal and opposite angles of attack of 5° and their tips separated by 0.25c they generated a flow within the test section containing all the phenomena of current interest – the interaction of distinct co-rotating vortices, merger, and the relaxation of the new core. Figure 2 shows the core trajectories for this configuration, which was selected for the velocity measurements. After being shed from the wings the two cores spiral around each other as a consequence of the interaction of their velocity fields. The cores move slightly apart and then together as this interaction brings them towards merger. Merger begins just downstream of $x/c = 20$ (see coordinate system, figure 1) after about 1.5 orbits of the vortex pair and occurs over a streamwise distance of about 2c. Note that the labels A and B, defined in figure 2(*a*) are used to distinguish the unmerged vortices throughout the remainder of this paper.

	$x/c = 10$, A	$x/c = 10$, B	$x/c = 15$, A	$x/c = 15$, B	$x/c = 22$	$x/c = 30$
r_1/c	0.039	0.039	$0.046^{-0.005}$	$0.046^{-0.008}$	0.107*	0.105
$V_{\theta 1}/U_\infty$	0.17	0.16	$0.15^{+0.02}$	$0.13^{+0.02}$	0.13*	0.13
U_D/U_∞	0.13	0.12	$0.11^{+0.01}$	$0.11^{+0.01}$	0.07	0.07
$2\pi r_1 V_{\theta 1}/U_\infty c$	0.042	0.039	0.043	0.038	0.087	0.086
d/c	0.302		0.225		—	—
σ_{max}/c	0.0082	0.0089	0.0170	0.0176	0.0084	0.0121
σ_{min}/c	0.0054	0.0055	0.0064	0.0062	0.0069	0.0080
θ_{max}(deg.)	78.5	77.6	−1.8	0.0	15.3	30.5

* Ignoring spiral arms.

TABLE 1. Circumferentially averaged core radii (r_1), peak tangential velocity ($V_{\theta 1}$) and centreline axial velocity deficit with approximate corrections for wandering at $x/c = 15$ (superscripted). Also, core circulations ($2\pi r_1 V_{\theta 1}/U_\infty c$), distance between vortex centres (d), principal RMS wandering amplitudes ($\sigma_{max}, \sigma_{min}$) and angle of the principle axis $\theta_{\max}$ measured from the y- toward the z-axis.

Hot-wire anemometry was used to make three-component velocity measurements in cross-sections through the unmerged vortices at $x/c = 10$ and 15, through the merger region at $x/c = 22$ and the merged vortex at $x/c = 30$. Measurements were made in polar grids (consisting of between 10 and 18 radial profiles) centred on the vortex cores. Profiles were also measured through the wake of the positive-y wing at $y/c = 2.5$ where the flow was very similar to a two-dimensional plane wake (see Zsoldos 1992). At each point 614 400 samples of the velocity vector were recorded in bursts at a rate of 30 kHz and over a total sampling time of about 2 minutes. Uncertainty estimates in measurements are given in table 3 of DLRF.

Miniature four-sensor hot-wire probes calibrated directly for flow angle were used (see Wittmer, Devenport & Zsoldos 1998). These sense the instantaneous velocity vector from within a 0.5 mm^3 measurement volume. Before using these probes it was necessary to demonstrate that they could be employed in and around the vortex cores without probe interference effects. Flow visualizations, velocity measurements and calculations were carried out to this end (see DLRF and Zsoldos 1992), all of which indicated that interference was not significant, in accord with the previous findings of Hoffmann & Joubert (1963) and Phillips & Graham (1984). Before interpreting the hot-wire data, it was also necessary to characterize any effects of vortex wandering. Wandering describes the low-frequency low-wavenumber side-to-side motions that seem to be an inevitable feature of wind-tunnel-generated tip vortices. The method of DLRF, which uses the intensity of low-frequency velocity fluctuations at the vortex centres and the mean-velocity fields of their cores, was used to quantify the wandering motions and their effects on mean velocity and turbulence measurements. This method gives estimates of the principle axes of the wandering motions (in the cross-flow plane) and the r.m.s. amplitude of the motions in those directions.

These results, listed in table 1, show wandering amplitudes at all stations to be only a small fraction of the vortex core diameters – a result supported by the flow visualizations of Zsoldos (1992). The wandering amplitudes are greatest at $x/c = 15$ where they are also most anisotropic. Merger quenches the anisotropic component of the wandering but amplitudes at $x/c = 22$ and 30 are still significant and appear to be growing with downstream distance.

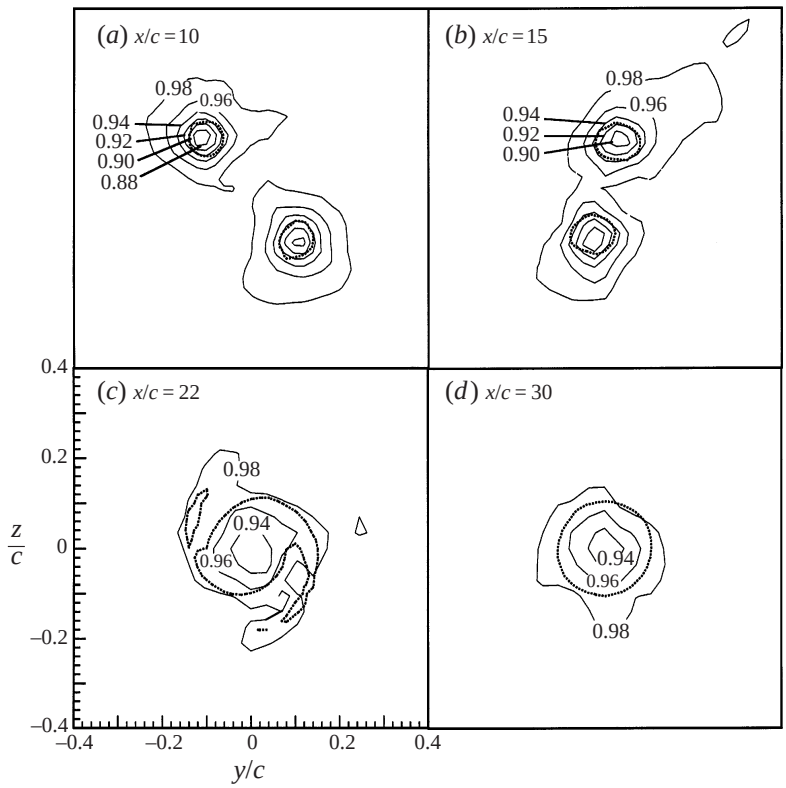

FIGURE 3. Contours of axial mean velocity U/U_∞. Dotted lines show core edges.

3. Results and discussion

The wing-fixed Cartesian coordinate system (x, y, z) (U, V, W) shown in figure 1 will be used to present most results. Velocities will also be presented using the cylindrical component V_θ, defined relative to the local vortex centreline. At $x/c = 10$ and 15, centreline orientations were inferred from the vortex trajectories of figure 2. Most of the results are normalized on the wing chord c of 0.203 m and the free-stream velocity U_∞ of about $20\,\mathrm{m\,s^{-1}}$.

3.1. *Mean flow field*

Mean-flow measurements are shown in figures 3 to 5 as contours of mean axial velocity, mean axial vorticity and mean tangential velocity. Vortex core parameters obtained from these measurements are listed in table 1. These measurements are not corrected for the smoothing effects of wandering. At all stations except $x/c = 15$, corrections were negligible compared to measurement uncertainty. At $x/c = 15$ sufficiently accurate corrections could not be made because the cores were not axisymmetric (an implicit assumption of DLRF's method). Instead estimated corrections are summarized in table 1 as approximate errors in core parameters.

At $x/c = 10$ the contours of mean axial vorticity (figure 4*a*) are dominated by the maxima associated with the vortex centres. The centres are separated by a distance of about $0.30c$ and the line joining them makes an angle of 135° with the y-axis, this being the approximate angle through which the vortices have spiralled since their

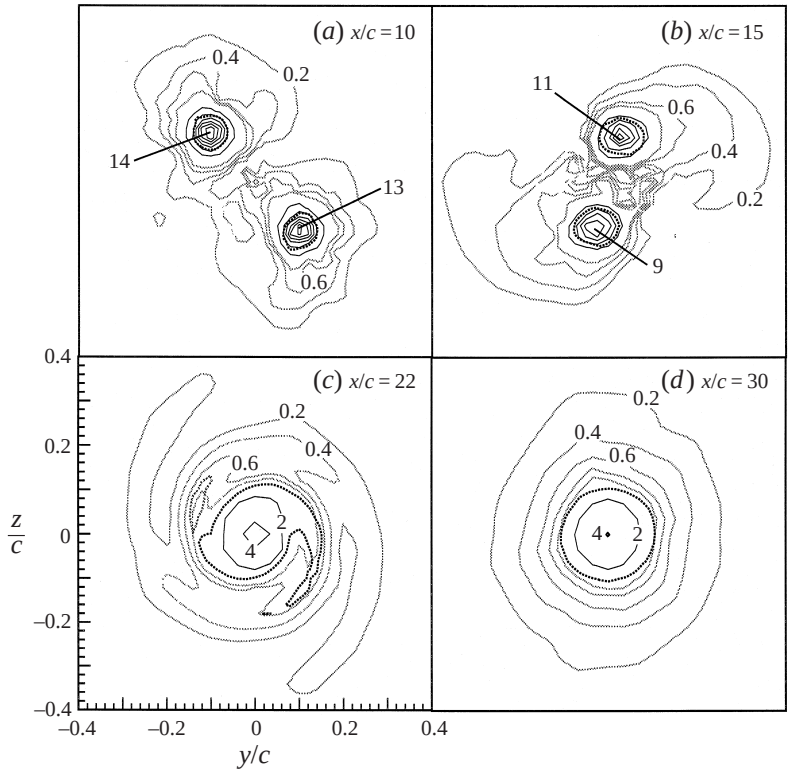

FIGURE 4. Contours of axial mean vorticity $\omega c/U_\infty$. Grey contours are in steps of 0.2, black contours in steps of 2. Dotted lines show core edges.

formation near the wing tips (see figure 2*b*). The tangential velocity fields resolved about these centres (figure 5*a*) reveal two circular cores $0.08c$ in diameter. The cores produce axial velocity deficits U_d (figure 3*a*) of about $13\%U_\infty$ and peak tangential velocities $V_{\theta 1}$ of about $16\%U_\infty$, with variations of about $\pm 1\%U_\infty$ around the edges (figure 5*a*). Integrating these variations we find that the cores each have a circulation Γ_1 of about $0.04U_\infty c$ – some 17% of the bound circulation on each wing Γ_0 (computed using lifting line theory adapted to account for both wings and the confining effects of the wind-tunnel walls).

Judging from the tangential velocity fields, fluid in the cores rotates about five times between $x/c = 10$ and 15. At the same time the vortices spiral around each other through a further 120° and their centres move about 25% closer (figure 4). The cores also become less axisymmetric. At $x/c = 15$ there is a $\pm 3\%$ U_∞ variation in the measured tangential velocity around the core edges with the highest velocities being found on the side closest to the centreline of the flow (figure 5*b*). The average peak tangential velocities are about $2\%U_\infty$ smaller than at $x/c = 10$, but there is little change in the core circulations, see table 1. The increase in wandering between $x/c = 10$ and 15 (see table 1) is sufficient to account for some of the measured decay in tangential velocity, but cannot explain the variations around the core edges. The wandering motions at $x/c = 15$ are directed primarily along the y-axis and thus smoothing of the tangential velocity field would have been greatest here. Peak tangential velocities on this axis are amongst the largest measured, however, suggesting that without wandering the azimuthal variations would appear

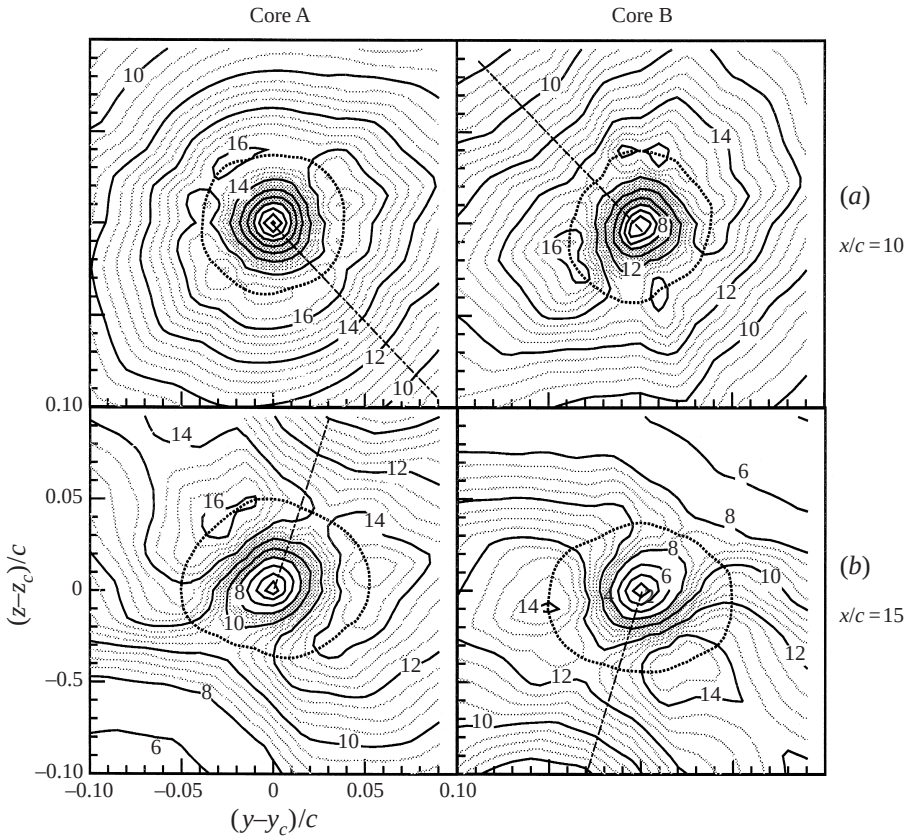

FIGURE 5. For caption see facing page.

even greater. Wandering may be partly responsible for the roughly elliptical shape of the cores seen in these measurements, longer in the y-direction (diameter $\sim 0.1c$) than in z (diameter $\sim 0.08c$). However, this may be partly a real effect too. As noted in the Introduction, several previous studies of two-dimensional vortex interaction show the formation of elliptical cores as a result of the strain rate field of one vortex acting upon the other.

The mean flow field outside the cores also evolves between $x/c = 10$ and 15. The regions of axial mean velocity deficit produced by the vortices (figure 3) begin to visibly merge as the cores approach each other. The distributions of mean streamwise vorticity become convected into regions that trail behind the spiralling cores (figure 4). The formation of these regions, known as filaments, is predicted in the two-dimensional simulations of Melander *et al.* (1988), Steger & Kutler (1977) and others, but as far as we are aware this is the first direct experimental observation in tip vortices. The filaments are thought to play a key role in the merger process since it is the velocities they induce that tend to move the vortex cores together.

The secondary velocity field responsible for the convection of vorticity and turbulence around the co-rotating vortex pair is illustrated in figure 6. This figure shows mean cross-flow velocity vectors plotted for a frame of reference rotating with the spiralling vortex pair. (Only in such a frame do they provide an indication of the particle paths of the mean flow). This has been done by adding a solid-body rotation about the flow centreline with an angular velocity equal to the orbit rate of the vor-

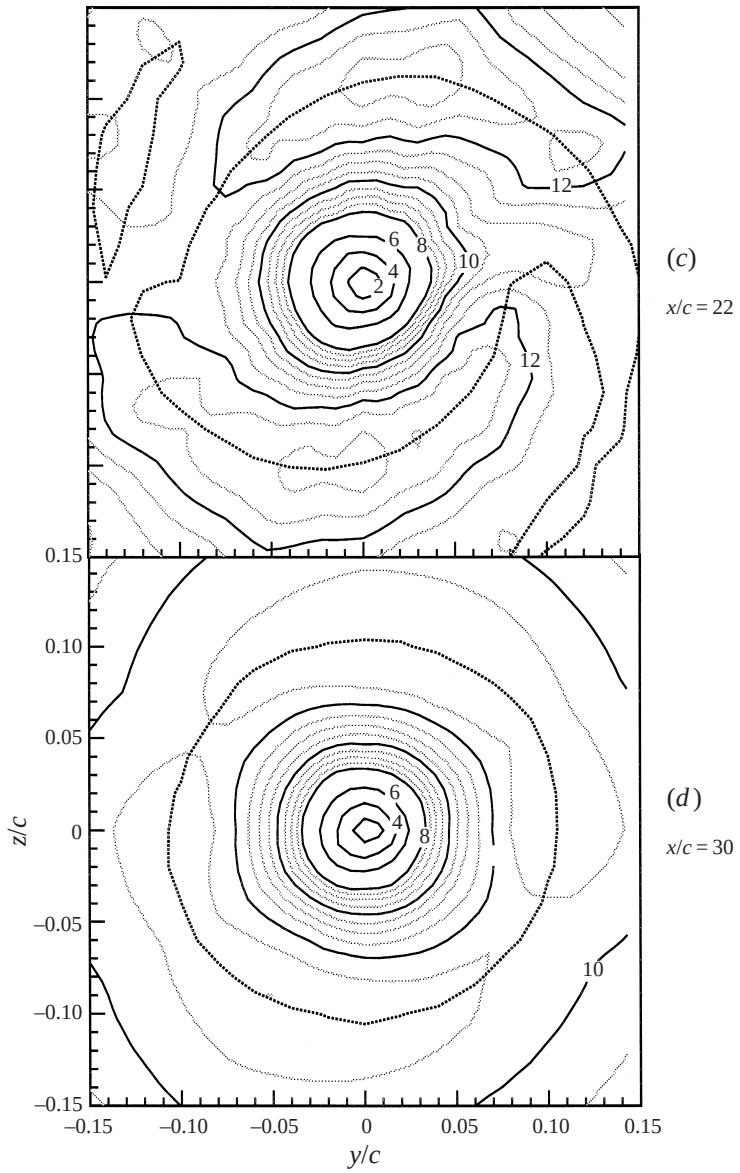

FIGURE 5. Contours of tangential mean velocity. Contour labels are percent U_∞. Dotted lines show core edges and chained lines join the core centres (and thus point to the flow centreline). Core labels A and B are defined in figure 2.

tices seen by an observer travelling with the free stream (inferred from figure 2*b*). To assist in interpretation of these pictures we have plotted alongside them the cross-flow streamline pattern produced by a pair of equal-strength ideal point vortices orbiting each other in an otherwise static field, as seen from a similar rotating frame. The vector fields show all the qualitative features of this potential flow model, namely the cross-flow stagnation points and corresponding multiple regions of circulating flow. There is also some quantitative agreement in the positions of these features, particularly the stagnation points. The stretching rates produced by the mean flow

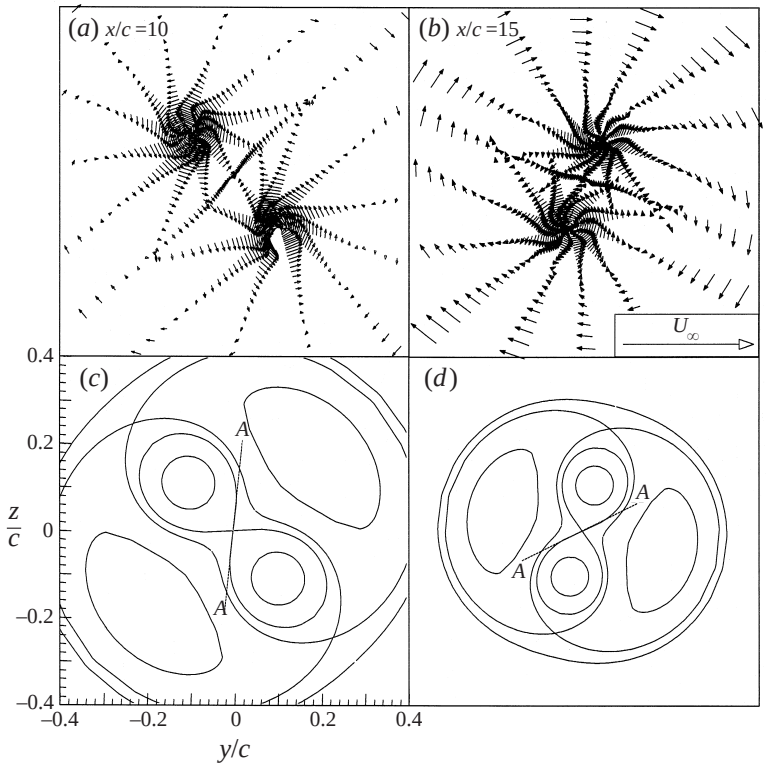

FIGURE 6. (*a*, *b*) Cross-flow mean-velocity vectors as seen from a frame of reference rotating with the vortices. (*c*, *d*) Cross-flow streamlines as seen in a frame of reference rotating with a pair of co-rotating ideal line vortices. Streamlines scaled to match actual vortex locations at $x/c = 10$ and 15.

around the centre stagnation point, and the exchange-band streamlines that pass around both vortices, turn out to be key features of this flow field from the point of view of understanding its turbulence structure.

Between $x/c = 15$ and 22, the vortices approach each other further and merger begins, the cores completing about one more orbit in the process. The mean velocity and vorticity measurements at $x/c = 22$ (figures 3*c* to 5*c*) reveal the new single core in the process of formation. The core displays almost perfect antisymmetry in its tangential mean velocity field (figure 5*c*). Peak tangential velocities are greatest (about $13\%U_\infty$) on a vertical cut through the core centre, and lowest (about $11\%U_\infty$) on a horizontal cut. The circumferential variations in the tangential velocity field imply a core shape resembling a spiral galaxy, consistent with prior two-dimensional simulations (e.g. Melander *et al.* 1988). The fact that the trailing arms of the core have a visible imprint in the mean-vorticity field (figure 4*c*), suggests that they are not just consequences of the resolution of the velocity field into a cylindrical system, but may truly be remnants of the co-rotating cores. Ignoring the spiral arms, the average core diameter is $0.107c$ and the total core area is $0.036c^2$ – about $2\frac{1}{2}$ times the combined area of the cores at $x/c = 15$ and $3\frac{1}{2}$ times that at $x/c = 10$. The new core must therefore be formed primarily from fluid not contained within the cores of the unmerged vortices. The circulation around the new core edge is $0.087U_\infty c$, only slightly greater than the combined circulation of the unmerged cores. The vorticity

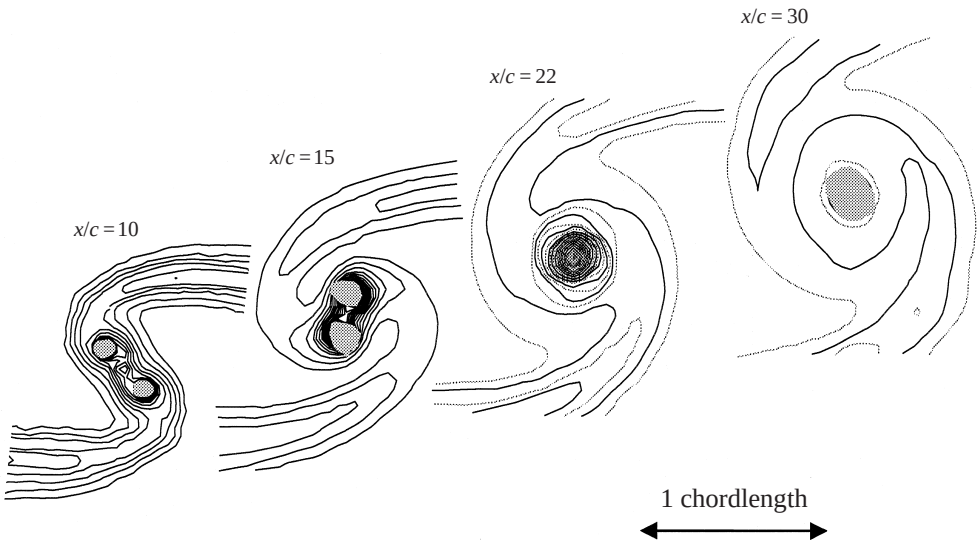

FIGURE 7. Contours of turbulence kinetic energy k/U_∞^2. Black contours in steps of 10^{-4}, grey contours at $x/c = 22$ and 30 show intermediate levels.

and axial velocity deficit at the core centre are one third to one half of the values seen in the unmerged cores at $x/c = 10$.

Between $x/c = 22$ and 30, the newly formed vortex relaxes to an almost axisymmetric state. The core edge becomes circular and the tangential velocity variations around it insignificant. At $x/c = 30$, the average peak tangential velocity at the core edge ($V_{\theta 1} = 0.13\,U_\infty$), the core diameter (0.105), the core strength ($\Gamma_1 = 0.086\,U_\infty c$) and centreline axial velocity deficit ($7\%U_\infty$), are almost identical to their values at $x/c = 22$. The lack of change in the flow parameters suggests that the new core is very stable. Stability would be expected given the monotonically increasing circulation distribution (Rayleigh's criterion) and low Rossby number $U_d/V_{\theta 1}$ (see Mayer & Powell 1992).

3.2. *Turbulence structure*

Figure 7 gives a broad view of the turbulence structure of the flow in terms of contours of turbulence kinetic energy $k = \frac{1}{2}(\overline{u^2} + \overline{v^2} + \overline{w^2})$. The shaded regions drawn on this figure indicate where wandering contributed more than 30% (according to the results of DLFR's method). We found wandering to be a dominant contributor to most turbulence quantities measured in the core of the vortex downstream of merger at $x/c = 30$ (but see below), suggesting that it may have been a factor in some previous studies of split-wing configurations.

Figure 7 reveals most clearly the development of the initially unrolled-up parts of the wing wakes and their attachment to the turbulent region containing the cores. Upstream of merger ($x/c = 10$ and 15), the wakes are distorted into spirals by the orbiting of the cores and the swirling velocity fields they produce. When the cores merge ($x/c = 22$) these combine to form a large turbulent region which then relaxes to a roughly axisymmetric state about $1.2c$ in diameter ($x/c = 30$). Outside the region directly influenced by the vortex cores overall turbulence levels decay quite rapidly with distance downstream. At a distance of $0.5c$ from the flow centreline, for example, the peak turbulence kinetic energy drops continuously from $0.0005U_\infty^2$ at

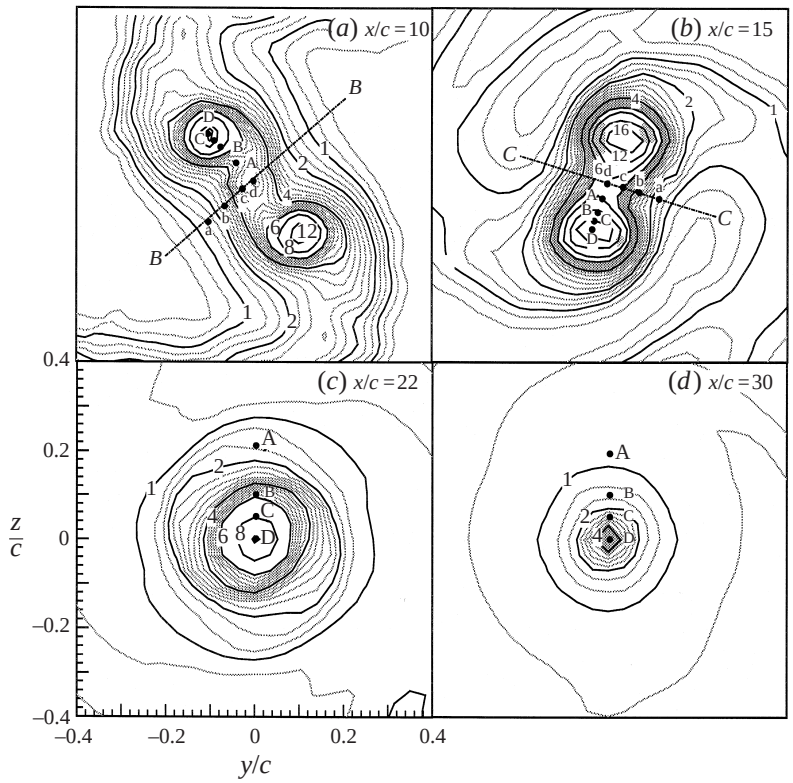

FIGURE 8. Contours of $\overline{u^2}/U_\infty^2 \times 10^5$, enlarged to show turbulence structure around the cores. Grey contours show evenly spaced intermediate levels. Shaded regions at $x/c = 15$ are where wandering is estimated to have contributed more than 30%.

$x/c = 10$ to 0.0001 U_∞^2 at $x/c = 30$ – about twice the rate of decay seen in the near two-dimensional part of the wake at $y/c = 2.5$ (Zsoldos 1992). The implication is that the distortion and roll-up of the wakes hastens their decay, see Vogel (1995) for discussion of this point.

Figure 8 gives a detailed view of the turbulent region surrounding the vortex cores in terms of contours of $\overline{u^2}/U_\infty^2$. This stress component is the least affected by wandering and, apart from some small regions near the core edges at $x/c = 15$, the measurements are free of substantial wandering effects. At $x/c = 10$ and 15 (figures 8*a* and 8*b*) the turbulence structure shows no sign of the separate wake spirals that must have originally surrounded each core nor the free-stream fluid that once separated them (this is in direct contrast to the counter-rotating vortex case, see DZV). The turbulent region is instead dominated by an 'S'-shaped braid of high turbulence levels that links the cores, reminiscent of that seen in Bilanin *et al.*'s (1977*b*) two-dimensional calculations. Turbulence levels in the braid actually increase with distance downstream, by about 40% between $x/c = 10$ and 15, in contrast to the rapid decay of the wake spiral turbulence.

This turbulence structure appears to be a consequence of the mean cross-flow velocity field between the vortices (figure 6). The absence of any remnants of the vortex-formation process can be explained as a result of the convection of turbulence along the exchange-band streamlines, which (at the secondary flow velocities measured) would rapidly combine the turbulence structure of the two vortices. The braid

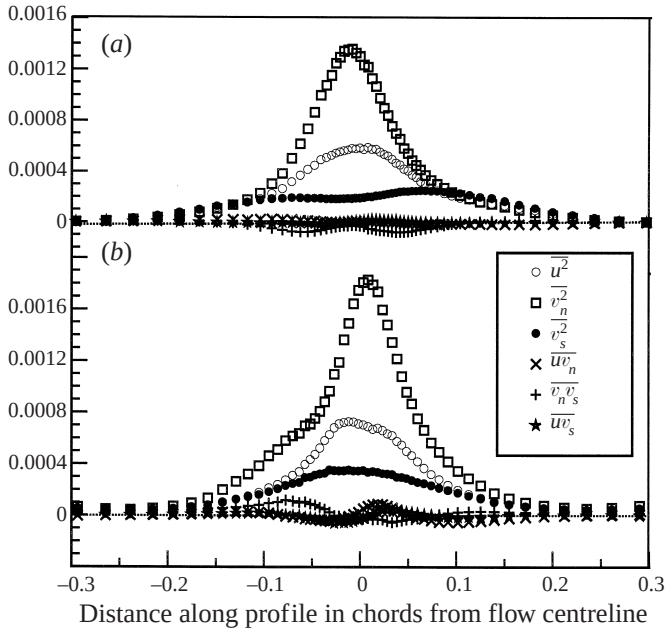

FIGURE 9. Profiles of turbulence stresses along plane of antisymmetry at (*a*) $x/c = 10$ and (*b*) 15, normalized on U_∞ (lines BB and CC, figure 8). Stresses resolved into components v_s and v_n parallel and normal to the stretching streamline AA in figures 6(*c*) and 6(*d*).

can be partly explained as a consequence of the mean rate of stretching experienced by the combined turbulence along the streamline AA that passes between the cores (figure 6). The principal axis of the strain rate tensor is aligned with AA over most of the region surrounding the flow centreline at $x/c = 10$ and 15. Mean stretching rates in this direction at the centreline, $\partial V_s/\partial s$, (where V_s and s are parallel to AA) are $1.2U_\infty/c$ at $x/c = 10$ and $1.7U_\infty/c$ at $x/c = 15$. For comparison the peak mean strain rate ($\partial U/\partial z$) in the un-rolled up part of the wake at $y/c = 2.5$ is about $0.4U_\infty/c$ at $x/c = 10$. One would expect (based upon studies such as Keffer 1965 and Mobbs 1968) this stretching to intensify any eddies aligned with the stretching direction, and attenuate other motions, resulting in anisotropy in the Reynolds stress tensor. Exactly this type of anisotropy is visible in turbulence stress profiles measured through the braid. Figure 9 shows stresses measured along the lines BB and CC (see figure 8) in terms of velocity components v_s and v_n, parallel and perpendicular to AA. Near the centre of the braid the normal stresses perpendicular to the stretching ($\overline{u^2}$ and $\overline{v_n^2}$) are between 2 and 6 times the stress $\overline{v_s^2}$ parallel to it, consistent with the expected behaviour of the eddies. In addition, the turbulence shear stresses are small, indicating that the principal axes of the stress tensor are almost perpendicular to the stretching streamline.

Velocity autospectra $G_{V_nV_n}$ measured in and around the braid suggest that this stretched turbulence may be organized in other ways. The spectra (figure 10) contain a peak centred at a frequency $fc/U_\infty \approx 3.7$ at $x/c = 10$, that becomes more distinct and falls in frequency to about $fc/U_\infty = 2.5$ at $x/c = 15$. This feature, which also appears in the U-spectra but is absent from V_s-spectra, would be consistent with the presence of a quasi-periodic train of eddies in the braid with axes aligned with the stretching direction. If we assumed these structures to be convected at the free-stream velocity, then the peak frequencies suggest an average spacing of $0.27c$ at $x/c = 10$

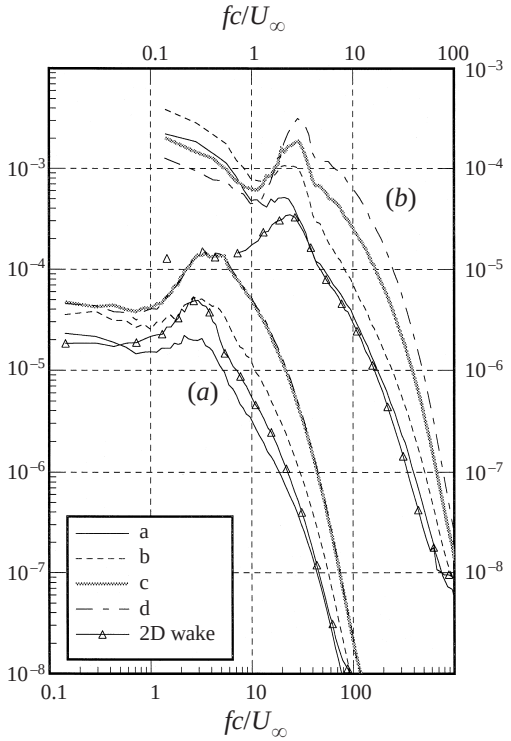

FIGURE 10. Autospectra $G_{V_nV_n}/U_\infty c$ of velocity fluctuations at (*a*) $x/c = 10$ and (*b*) 15 at points a to d marked on figure 8, compared with autospectra $G_{WW}/U_\infty c$ measured at $y/c = 2.5$ on the centreline of the near two-dimensional part of the wake (Zsoldos 1992).

and $0.4c$ at $x/c = 15$, equivalent to 0.9 and 1.8 times the local vortex separation respectively.

Why does the braid turbulence appear to be organized in this way and why do braid turbulence levels increase with distance downstream? One possibility is instability of the velocity field between the vortices (figure 6). In transitional mixing layers a very similar field, formed between adjacent spanwise rollers, is responsible for the Pierrehumbert–Widnall (1982) instability. This instability skews vorticity from the rollers into the streamwise direction where it becomes organized into counter-rotating eddies that, again, form a braid (e.g. Lasheras, Cho & Maxworthy 1986). The present braid is not only similar in shape and relative position to such mixing-layer braids (Corcos & Lin 1984; Metcalfe *et al.* 1987) but the structure spacings we have inferred from spectra are comparable to the counter-rotating eddy spacings seen in mixing-layer braids (Lasheras *et al.* 1986; Ragab, Sheen & Sreedhar 1992; Metcalfe *et al.* 1987).

One interesting characteristic of Pierrehumbert–Widnall instability is that its growth rate varies only gradually with wavenumber. The spacing of the braid structures it produces is thus extremely sensitive to flow conditions (e.g. Bernal & Roshko 1986). One might therefore expect, in the absence of any other stimulus, the weak but quasi-periodic turbulent motions in the spiral wakes surrounding the vortices to organize the formation of eddies in the braid. Indeed such a mechanism is suggested by the resemblance between the braid spectra and spectra measured in the unrolled-up parts of the wakes, samples of which are included in figure 10. The peak in the braid spectra occurs

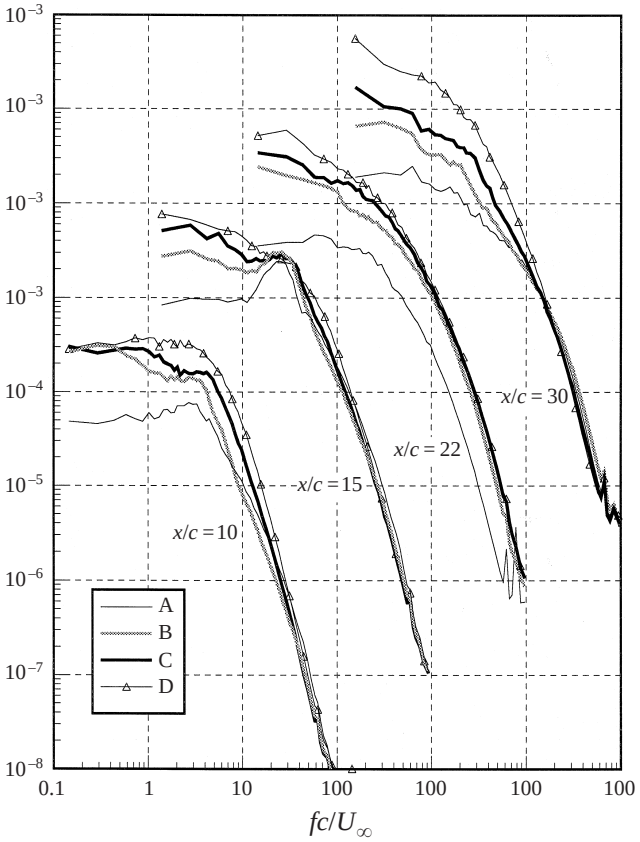

FIGURE 11. Autospectra $G_{UU}/U_\infty c$ of velocity fluctuations at points A to D marked on figure 8 for all streamwise stations.

close to the frequency of the peak in the wake spectra at both $x/c = 10$ and 15, the two frequencies falling by the same proportion over the intervening streamwise distance.

We now turn our attention to the cores of the unmerged vortices, where the measured turbulence normal stresses rise to their maximum values (figure 8). While wandering is not a dominant contributor to $\overline{u^2}$, the large values of this stress inside the cores do not necessarily indicate intense turbulent mixing. As suggested by DLRF and DZV and confirmed by Youssef *et al.* (1998), velocity fluctuations in the core may result from inactive motions as it is buffeted by surrounding turbulence. The various contributions to the velocity fluctuations measured in and around the vortex cores may be distinguished to a degree by examining velocity spectra. Figure 11 includes autospectra of U fluctuations measured at representative points A, B, C and D (defined at both $x/c = 10$ and 15, see figure 8) that extend in radial profiles from the braid region to the centre of vortex A. At low frequencies ($fc/U_\infty < 1$) spectral levels increase as the core is approached and entered as a result of the wandering. At mid frequencies ($1 < fc/U_\infty < 20$) there is a broadband increase, perhaps as a result of the inactive motion mentioned above, and spectra measured both outside (points A and B) and inside (point C) the core show signs of the same spectral peaks seen at the braid centreline (at frequencies of $fc/U_\infty = 3.7$ and 2.5 for $x/c = 10$ and 15).

At high frequencies ($fc/U_\infty > 20$) the spectrum should be dominated by contributions from the smaller turbulence scales. In the laminar core of the single tip vortex

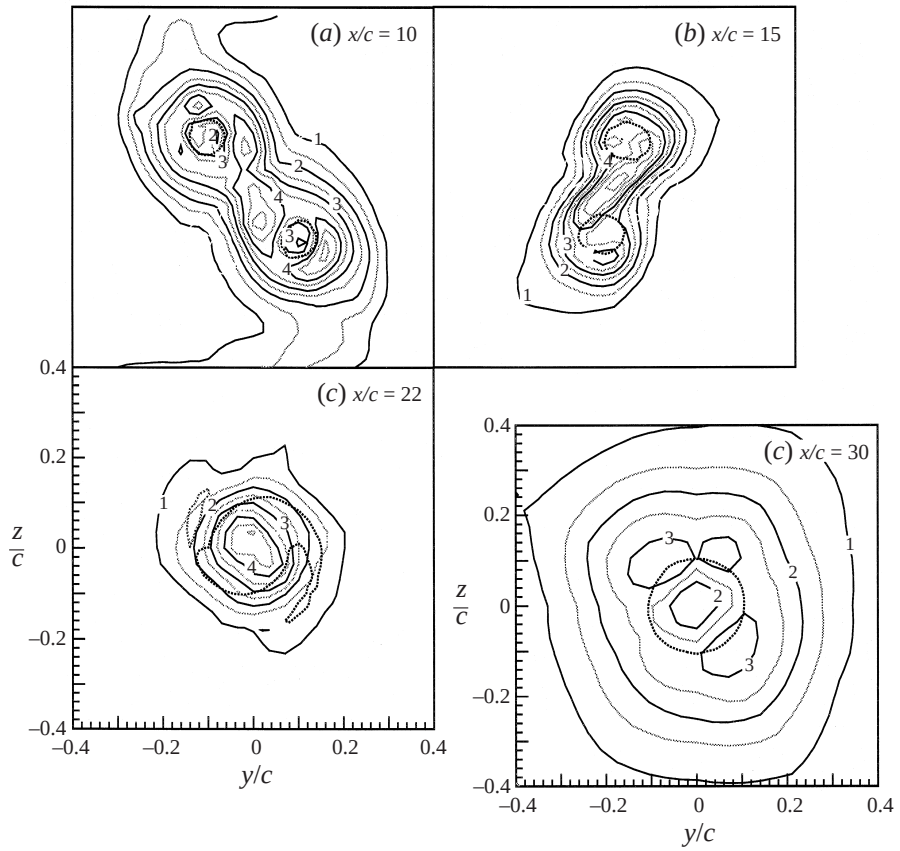

FIGURE 12. Contours of $\overline{u^2}/U_\infty^2 \times 10^6$, high-pass filtered at $fc/U_\infty = 40$ (*a*, *b* and *c*) and $fc/U_\infty = 25$ (*d*).

studied by DLRF, velocity spectra showed an order of magnitude less energy at high frequencies than in the surrounding wake spiral. The same behaviour is not seen in here (figure 11). High-frequency spectral levels at the core centre (point D) and edge (point C) are comparable to those measured in the adjacent turbulent braid (point A) and considerably larger than those on the centreline of the unrolled-up wake. The implication is that the co-rotating cores are turbulent. Given that the spectral feature associated with the braid appears in the cores, we speculate that this turbulence is one consequence of the braid instability.

The cross-sectional structure of the cores in this high-frequency range can be seen by high-pass filtering the turbulence stress fields, performed in the Fourier domain by integrating the energy above the cutoff frequency. Figure 12 shows contours of $\overline{u^2}$ filtered at $fc/U_\infty = 40$. At $x/c = 10$ high-frequency velocity fluctuations are at their most intense in the braid region that joins and appears to partially circle both cores. The cores are marked by slight depressions in the filtered stress field presumably because of the stabilizing effects of their rotation, but these do not compare to the more than 5-fold reduction in small-scale turbulence levels found in the laminar core of the isolated vortex (DLRF). At $x/c = 15$ small-scale turbulence levels in the braid region are undiminished and the braid region appears to overlap the core edges. Levels near the core centres are slightly depressed, but the overall influence of the cores on the stress field is much less marked.

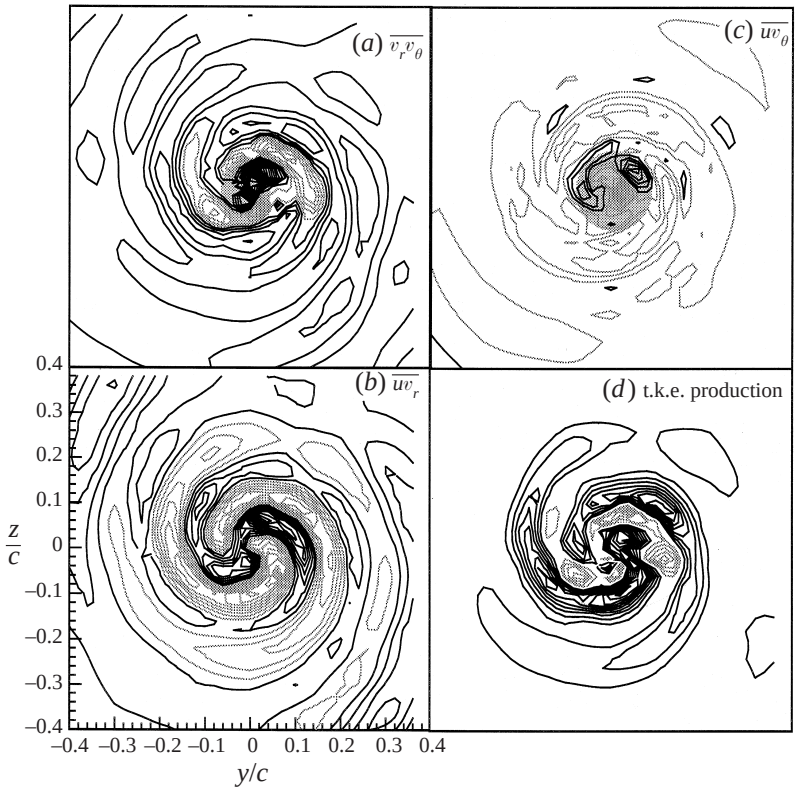

FIGURE 13. (*a–c*) Contours of turbulence shear stresses in terms of cylindrical components at $x/c = 22$. Contour spacing $10^{-5}\,U_\infty^2$. (*d*) Contours of t.k.e. production at $x/c = 22$. Contour spacing $5 \times 10^{-6}\,U_\infty^3/c$. Grey contours show negative levels. Black contours show zero and positive levels. Shaded regions are where wandering is estimated to have contributed more than 30%.

The rapid orbiting of the vortices that accompanies the merger wraps the outer parts of the wakes, the turbulence that surrounds the cores, into a tight double spiral. At $x/c = 22$ this spiral forms a single turbulent region 1.2 chordlengths diameter (figure 7). Merger also quenches the anisotropic component of the wandering motions (table 1) and produces a decrease in cross-stream velocity gradients, all but eliminating wandering contributions to the turbulence stresses. As a result we are able to plot for $x/c = 22$ meaningful contours of $\overline{uv_r}$, $\overline{uv_\theta}$, $\overline{v_r v_\theta}$ and turbulence kinetic energy (t.k.e.) production (computed ignoring streamwise derivatives), figure 13.

The spiral structure of the turbulent region containing the new core is most clearly revealed in the $\overline{uv_r}$ contours which show bands of positive and negative shear stress that run all the way to the centre of the newly formed core. A similar pattern is also visible in $\overline{v_r v_\theta}$, and to a lesser extent in $\overline{uv_\theta}$, which is easily the smallest of the three shear stresses. A double spiral with both positive and negative regions is also visible in the t.k.e. production – the negative regions being coincident with the spiral arms of the new core. The largest contributor to the production over most of the cross-section is

$$-\tfrac{1}{2}\overline{v_r v_\theta}\left(\frac{\partial V_\theta}{\partial r} - \frac{V_\theta}{r} + \frac{1}{r}\frac{\partial V_r}{\partial \theta}\right),$$

associated with the radial mixing of angular momentum. This term, which shows a distribution very similar to the total production, becomes negative because of the

negative excursions of $\overline{v_r v_\theta}$ found near the edge and in the tails of the new core. Some negative contributions also come from

$$-\tfrac{1}{2}\,\overline{uv_r}\,\frac{\partial U}{\partial r},\ -\tfrac{1}{2}\,\overline{v_r^2}\,\frac{\partial V_r}{\partial r} \quad \text{and} \quad -\tfrac{1}{2}\,\overline{v_\theta^2}\left(\frac{1}{r}\frac{\partial V_\theta}{\partial \theta}+\frac{V_r}{r}\right).$$

The complex flow structure generated by merger decays rapidly with downstream distance to a nearly axisymmetric and relatively featureless form. By $x/c = 30$ the contours of $\overline{u^2}$ (figure 8*d*) form almost perfect circles around the core and the turbulence shear stresses in and around the core have dropped to such low values that their contours (not shown) show little but measurement uncertainty. The turbulence kinetic energy distribution (figure 7) shows some lingering asymmetry in the core region, but this appears to be the result of contributions from the anisotropic wandering motions at this station. It is interesting to note how different the turbulence structure at $x/c = 30$ is from that which forms around a comparable single wing-tip vortex. A comparison of figure 7 with figure 7 of DLRF shows that the tip vortex shed from a single wing produces a much smaller, less axisymmetric turbulent region. While it is fairly obvious that split-wing vortices and wing-tip vortices should have a different turbulence structure this is, as far as the authors are aware, the first quantitative comparison demonstrating how large those differences are.

Inside the core at $x/c = 22$ and 30 velocity fluctuation levels increase monotonically to the vortex centre. The $\overline{u^2}$ levels at the centre (barely influenced by wandering) are 0.00107 and 0.00061 at $x/c = 22$ and 30 – 'turbulence' intensities of 3.3 and 2.5% respectively. The nature of these velocity fluctuations is to some extent visible in the U-component velocity spectra measured at different radial locations, as shown in figure 11. At both $x/c = 22$ and 30, the spectra are quite similar in the region of turbulence rolled up by the merger process (points A) where they have a broad-band form fairly typical of wake-type turbulent flows. Both sets of spectra also show the same rise in low- and mid-frequency ($fc/U_\infty < 20$) spectral levels as the core is approached and entered. The behaviour at high frequencies (say $fc/U_\infty > 20$), however, where we expect to see fluctuations produced by smaller-scale turbulence, is quite different. At $x/c = 22$ the intensity of high-frequency velocity fluctuations increases to its maximum value at the core centre, suggesting the presence of turbulence too active to be quenched by the stabilizing rotation of the core. At $x/c = 30$, high-frequency velocity fluctuations reach their maximum intensity near the core edge (point C) indicating, perhaps, that the new core is returning to a more stable form. Absent from either set of spectra (or others measured at different azimuthal angles) are any obvious remnants of the braid turbulence, consistent with the hypothesis that this turbulence is generated and organized by the strain rate field between the two orbiting vortex cores.

The cross-sectional structure of the core in this high-frequency range is shown in figure 12. At $x/c = 22$, contours of $\overline{u^2}/U_\infty^2$ high-pass filtered at $fc/U_\infty = 40$ reveal a structure opposite to that of the laminar core of a single tip vortex (DLRF), with high-frequency spectral levels being at their greatest in the core centre. The peak filtered stress, 4.5×10^{-6}, is almost as large as that seen in the middle of the braid at $x/c = 15$. Downstream of $x/c = 22$ these filtered stress levels decay rapidly and by $x/c = 30$ are indistinguishable from the uncertainty. This rapid re-stabilization of the flow is remarkable, but leaves us with little insight into the structure of the relaxing core. This structure can, however, be revealed by slightly reducing the filter frequency, which we have done to produce the contours of figure 12(*d*). These stresses, high-pass

filtered at $fc/U_\infty = 25$, show a flow structure much more like that of the single tip vortex. High-frequency velocity fluctuations are largest in a ring surrounding the core edge and are depressed by almost a factor of two at its centre. It appears therefore that the core may be relaxing toward a laminar state downstream of merger.

4. Conclusions

Experiments have been performed on a co-rotating wing-tip vortex pair generated using two rectangular NACA 0012 wings in a split-wing configuration. Mean-velocity and turbulence measurements were made using hot wires. The small-amplitude wandering motions of the vortices were quantified, and their effects on the results accounted for using the method of Devenport *et al.* (1996). The measurements reveal, for the first time, the complex turbulence structure of this flow.

The vortices spiral around each other and merge some 20 chordlengths downstream of the generating wings. As merger is approached the vortices lose their axisymmetry – their cores develop lopsided tangential velocity fields and take on an elliptical appearance. The formation of filaments in the vorticity field, previously predicted for analogous two-dimensional vortex interactions, is also seen. The cores become part of a single turbulence structure long before they merge, as a result of the convection of turbulence between them by their combined cross-flow velocity field. This velocity field also stretches the turbulence, organizing it into an 'S'-shaped braid that links the cores. Consistent with stretching, turbulence stresses in the braid are highly anisotropic. They also increase with downstream distance. The braid quite closely resembles the structure formed between adjacent spanwise rollers in transitional mixing layers through the Pierrehumbert–Widnall instability. Velocity spectra measured in the braid show peaks consistent with the presence of secondary eddies analogous to those found in mixing layers, and spectra and filtered statistics suggest that these eddies extend well into the vortex cores. Consistent with the broadband nature of the Pierrehumbert–Widnall instability, it appears that the weak but quasi-regular motions present in the unrolled-up parts of the wing wakes may organize the formation of eddies in the braid. Unlike a single tip vortex, the unmerged cores of the co-rotating vortex pair appear to be turbulent. Filtered statistics show small-scale turbulence levels here comparable to or greater than peak levels in the surrounding flow.

The merging of the vortices wraps the cores and the flow structure that surrounds them into a large turbulent region with an intricate double-spiral structure, visible in the turbulence shear stresses, turbulence kinetic energy production, and the shape of the new single core. The new core, formed primarily from fluid outside the cores of the unmerged vortices, appears to be an initial focus of turbulent activity since high-frequency velocity fluctuations are at their most intense at its centre. The flow rapidly relaxes, however. The core and the turbulent field containing it become axisymmetric and the spectral content of the velocity fluctuations it produces becomes much more like that of the laminar core of a single wing-tip vortex. However, the large turbulent region formed around the vortex core during the merger process remains quite different than that found around a single tip vortex.

The experimental data presented in this paper may be accessed over the World Wide Web at http://www.aoe.vt.edu/flowdata.html.

The authors would like to thank Michael Rife and Gautam Sharma for their assistance in taking many of the above measurements, Dr Stewart Glegg of Florida Atlantic University for his contribution to the development of theory of wandering

effects, and DARPA for their financial support through ONR contracts N00014-90-J-1909 and N00014-91-J-1773, administered by Mr Gary W. Jones.

REFERENCES

Bandyopadhyay, P. R., Stead, D. J. & Ash, R. L. 1991 Organized nature of a turbulent trailing vortex. *AIAA J.* **29**, 1627–1633.

Bernal, L. P. & Roshko, A. 1986 Streamwise vortex structure in plane mixing layers. *J. Fluid Mech.* **170**, 499–525.

Bilanin, A. J., Snedeker, R. S. & Teske, M. E. 1976 Interactions and merging of between line vortices. *AFOSR-TR*-76-0873.

Bilanin, A. J., Teske, M. E., Donaldson, C. duP. & Snedeker, R. S. 1977*a* Viscous effects in aircraft trailing vortices. In *Wake-Vortex Minimization*, NASA SP409.

Bilanin, A. J., Teske, M. E. & Williamson, G. G. 1977*b* Vortex interactions and decay in aircraft wakes. *AIAA J.* **15**, 250–260.

Brandt, S. A. & Iversen, J. D. 1977 Merging of aircraft trailing vortices. *J. Aircraft* **14**, 1212–1230.

Christiansen, J. B. & Zabusky, N. J. 1973 Instability, coalescence and fission of finite area vortex structures. *J. Fluid Mech.* **61**, 219–243.

Corcos, G. M. & Lin, S. J. 1984 The mixing layer: deterministic models of a turbulent flow. Part 2. The origin of the three-dimensional motion. *J. Fluid Mech.* **139**, 67–95.

Corsiglia, V. R., Iversen, J. D. & Orloff, K. L. 1978 Laser-velocimeter surveys of merging vortices in a wind tunnel. *J. Aircraft* **15**, 762–768.

Devenport, W. J., Rife, M., Liapis, S. & Follin, G. J. 1996 The structure and development of a wing-tip vortex. *J. Fluid Mech.* **312**, 67–106 (referred to herein as DRLF).

Devenport, W. J., Zsoldos, J. S. & Vogel, C. M. 1997 The structure and development of a counter-rotating wing-tip vortex pair. *J. Fluid Mech.* **312**, 67–106 (referred to herein as DZV).

Dritschel, D. G. 1995 A general theory for two-dimensional vortex interactions. *J. Fluid Mech.* **293**, 269–303.

Hoffmann, E. F. & Joubert, P. N. 1963 Turbulent line vortices. *J. Fluid Mech.* **16**, 395–411.

Iversenn, J. D., Corsiglia, V. R., Park, S., Backhus, D. R. & Brickman, R. A. 1979 Hot-wire, laser-anemometer, and force measurements of interacting trailing vortices. *J. Aircraft* **16**, 448–454.

Keffer, J. F. 1965 The uniform distortion of a turbulent wake. *J. Fluid Mech.* **22**, 135–159.

Lasheras, J. C., Cho, J. U. S. & Maxworthy, T. 1986 On the origin and evolution of streamwise vortical structures in a plane, free shear layer. *J. Fluid Mech.* **172**, 231–258.

Mayer, E. W. & Powell, K. G. 1992 Similarity solutions for viscous vortex cores. *J. Fluid Mech.* **238**, 487–507.

Melander, M. V., Zabusky, N. J. & McWilliams, J. C. 1988 Symmetric vortex merger in two dimensions: causes and conditions. *J. Fluid Mech.* **195**, 303–340.

Metcalfe, R. W., Orszag, S. A., Brachet, M. E., Menon, S. & Riley, J. J. 1987 Secondary instability of a temporally growing mixing layer. *J. Fluid Mech.* **184**, 207–243.

Mobbs, F. R. 1968 Spreading and contraction at the boundaries of free turbulent flows. *J. Fluid Mech.* **33**, 227–239.

Moore, D. W. & Saffman, P. G. 1971 Structure of a line vortex in an imposed strain. In *Aircraft Wake Turbulence and its Detection* (ed. J. H. Olsen, A. Goldburg & M. Rogers), pp. 339–354. Plenum.

Overman, E. A. & Zabusky, N. J. 1982 Evolution and merger of isolated vortex structures. *Phys. Fluids* **25**, 1297–1305.

Pierrehumbert, R. T. & Widnall, S. E. 1982 The two and three-dimensional instabilities of a spatially periodic shear layer. *J. Fluid Mech.* **114**, 59–82.

Phillips, W. R. C. & Graham, J. A. H. 1984 Reynolds stress measurements in a turbulent trailing vortex. *J. Fluid Mech.* **147**, 353–371.

Poppleton, E. D. 1971 Effect of air injection into the core of a trailing vortex. *J. Aircraft*, August 1971, pp. 672–673.

Ragab, S. A., Sheen, S.-C. & Sreedhar, M. 1992 An investigation of finite difference methods for large-eddy simulation of a mixing layer. *AIAA Paper* 92-0554.

Rossow, V. J. 1977*a* Convective merging of vortex cores in lift-generated wakes. *J. Aircraft* **14**, 283–290.

Rossow, V. J. 1977*b* Inviscid modeling of aircraft trailing vortices. In *Wake-Vortex Minimization*, *NASA* SP409.

Smits, A. J. & Kummer, R. P. 1985 The interaction and merging of two turbulent line vortices. *AIAA Paper* 85-0046.

Steger, J. L. & Kutler, P. 1977 Implicit finite-difference procedures for the computation of vortex wakes. *AIAA J.* **15**, 581–590.

Vogel, C. M. 1995 The source and evolution of turbulence in trailing vortex pairs. MS thesis, AOE Dept. VPI & SU, Blacksburg, VA.

Wittmer, K. S., Devenport, W. J. & Zsoldos, J. S. 1998 A four-sensor hot-wire probe system for three-component velocity measurements. *Exps. Fluids* **24**, 416–423.

Youssef, K., Ragab, S., Devenport, W. & Abdel Gawad, A. 1998 Large eddy simulation of the near wake of a rectangular wing. *AIAA Paper* 98-0317.

Zsoldos, J. S. 1992 An experimental investigation of interacting wing-tip vortex pairs. MS thesis, AOE Dept. VPI & SU, Blacksburg, VA.